

Electron bremsstrahlung angular distributions in the 1–500 keV energy range

H. K. Tseng,* R. H. Pratt, and C. M. Lee†

Department of Physics and Astronomy, University of Pittsburgh, Pittsburgh, Pennsylvania 15260

(Received 16 June 1978)

Predictions of bremsstrahlung angular distributions from incident electrons of kinetic energy 1–500 keV are examined using numerical data obtained from a numerical calculation in partial waves, under the assumption that the process is described as a single-electron transition in an atomic central potential. For low- Z elements the Born approximation or the Elwert-Haug approach, modified with form-factor screening, give good predictions for the shape of the angular distributions, except at forward and backward angles. That is, the results are good in the main region which contributes to the energy spectrum. For high- Z elements such predictions are accurate within about 15%. Analytic properties of the shape of the angular distribution from simpler theories suggest a simple way to parametrize the results.

I. INTRODUCTION

The continuing improvement of computational capabilities has made it possible to obtain fairly accurate theoretical predictions^{1,2} for the electron bremsstrahlung spectrum from incident electrons with kinetic energies in the range of keV. This has coincided with increased need for such data, as in radiation physics³ and in controlled thermonuclear research.⁴ There is also some need for bremsstrahlung angular distributions for the same purposes. Here we wish to report predictions for the shapes of bremsstrahlung cross sections differential in photon energy and angle, to supplement our previous report² on the bremsstrahlung energy spectra, for incident electrons of kinetic energy from 1 to 500 keV.

Again in this report, our results are obtained by calculations in partial-wave expansions.¹ The bremsstrahlung process is described as a single-electron transition in a relativistic self-consistent central potential. Here we use the Kohn-Sham potential.⁵ We have verified that, in the energy range considered in this report, results are not sensitive to the detailed choice of the self-consistent central potential. However, for incident electron energies below 1 keV, this choice, as well as many-electron effects, becomes increasingly important.

In Sec. II, we will examine simpler theories for the shape function S , using the results obtained from our partial-wave calculations. This shape function of the bremsstrahlung angular distribution is defined as

$$S\left(Z, T_1, \frac{k}{T_1}, \theta\right) \equiv \frac{d\sigma}{dk d\Omega_k} / \frac{d\sigma}{dk}. \quad (1.1)$$

For a specific atomic target, the shape function S depends on the atomic number Z , the kinetic energy of incident electrons T_1 , the fractional energy

loss k/T_1 due to radiation of a photon of energy k , and the photon angle θ with respect to the incident-electron momentum \vec{p}_1 . The shape function is normalized so that

$$\int S d\Omega_k = 1. \quad (1.2)$$

Thus, our results for the shape function S along with the data for the bremsstrahlung energy spectra $d\sigma/dk$ published previously determine the electron bremsstrahlung angular distributions $d\sigma/dk d\Omega_k$.

In Sec. III, we discuss how best to represent or characterize the shape functions.

II. PREDICTIONS FROM SIMPLER THEORIES

We begin with the case of a point-Coulomb potential model for the target atom, which is generally assumed in simpler approximate theories, and afterwards examine the screening effects due to atomic electrons resulting from a screened central potential.

A simple result for the shape function^{6,7} is obtained from the nonrelativistic (NR) dipole approximation of Sommerfeld⁸

$$S_{\text{NR}} \propto 1 + \frac{1}{2} a_2 P_2(\cos\theta), \quad (2.1)$$

where a_2 is the particle parameter defined by Eq. (6) of Ref. 6. The same form, with a more general choice of a_2 , also holds for the screened case in the NR dipole approximation. In the NR dipole approximation, the bremsstrahlung matrix element has the simple form

$$M_{fi} \propto \int \psi_f^* \vec{\epsilon}^* \cdot \vec{r} \psi_i d^3r. \quad (2.2)$$

That is, $|M_{fi}|^2$ must be quadratic in $\vec{\epsilon}$, the polarization of the photon. If one integrates $|M_{fi}|^2$ over scattered-electron angles, the only other vector in

$\int |M_{fi}|^2 d\Omega_2$ is \vec{p}_1 , the momentum of the incident-electron. Remembering that $|\vec{\epsilon}|^2 = 1$, the only dependence of the scalar quantity $\int |M_{fi}|^2 d\Omega_2$ on the direction \vec{p}_1 is of the form $a + b |\vec{p}_1 \cdot \vec{\epsilon}|^2$, where a and b depend on Z , T_1 , and k/T_1 , but not on direction. This shows that the shape function, even for polarized photons, only depends on one parameter. Averaging over photon polarization we have

$$|\vec{p}_1 \cdot \vec{\epsilon}|^2 = \frac{1}{2} (\hat{k} \times \hat{p}_1)^2, \quad (2.3)$$

so that the general form of the shape function in the NR dipole approximation is given by Eq. (2.1). Here $\hat{k} = \vec{k}/k$, and $\hat{p}_1 = \vec{p}_1/p_1$.

Corrections to nonrelativistic dipole approximation result both from relativistic effects and from higher multipoles. There are relativistic corrections to wave functions in $Z\alpha \equiv Ze^2/\hbar c$ as well as in the electron velocity $\beta \equiv v/c$, so that in addition to modifications at relativistic energies there can be modifications in heavy elements persisting to very low energies. For the bremsstrahlung energy spectrum $d\sigma/dk$ cancellation² between higher multipole and relativistic corrections to the NR dipole approximation occurs for the incident electron energies T_1 below about 50 keV, extending the useful range of the NR dipole result. This cancellation does not occur for the angular distribution⁹ at keV energies and above, as we shall see. In relativistic dipole approximation, summing

and averaging electron spins, it is clear that the previous argument for the general form of the shape function still applies. Hence any deviations from this symmetric form are due to the inclusion of higher multipoles.

The multipole expansion is an expansion in powers of $\vec{k} \cdot \vec{r}$. Retracing the previous argument with these additional vectors \vec{k} , it is clear that the cross term from the l th multipole will contain additional angular dependence through $\cos^l \theta$, leading to nonvanishing B 's through B_{2+l} , if the shape function is characterized by the coefficients B_n in a Legendre expansion

$$S = \frac{1}{4\pi} \sum_{n=0}^{\infty} B_n P_n(\cos \theta) \quad (2.4)$$

with $B_0 \equiv 1$. In particular, the first multipole correction will give corrections to the shape function proportional to $\hat{k} \cdot \hat{p}_1 = \cos \theta$ or

$$S = \frac{1}{4\pi} \sum_{l=0}^3 B_l P_l(\cos \theta). \quad (2.5)$$

It has only been possible to obtain results in analytic form that go beyond dipole approximation for a few limiting cases. The best known such theory is the relativistic Born approximation of Bethe and Heitler,¹⁰ requiring $\nu = Z\alpha/\beta \ll 1$. In this approximation the shape function has the form, independent of $Z\alpha$,

$$S_B = (8\pi M\Delta)^{-1} \left[\frac{8(2E_1^2 + 1) \sin^2 \theta}{p_1^2 \Delta^3} - \frac{2(5E_1^2 + 2E_1 E_2 + 3)}{p_1^2 \Delta} - \frac{2(p_1^2 - k^2)}{Q^2 \Delta} + \frac{4E_2}{p_1^2} + \frac{L}{p_1^3 p_2} \right. \\ \times \left(\frac{4E_1(3k - p_1^2 E_2) \sin^2 \theta}{\Delta^3} + \frac{4E_1^2(E_1^2 + E_2^2)}{\Delta} + \frac{2 - 2(7E_1^2 - 3E_1 E_2 + E_2^2)}{\Delta} + 2k(E_1^2 + E_1 E_2 - 1) \right) \\ \left. - \frac{8}{p_2} \ln(E_2 + p_2) + \frac{\ln(Q + p_2)/(Q - p_2)}{p_2 Q} \left(\frac{4}{\Delta} - 6k - \frac{2k(p_1^2 - k^2)}{Q^2} \right) \right], \quad (2.6)$$

where

$$M = \frac{4}{3} - 2E_1 E_2 \frac{p_2^2 + p_1^2}{p_2^2 p_1^2} + \frac{\epsilon_1 E_2}{p_1^3} + \frac{\epsilon_2 E_1}{p_2^3} - \frac{\epsilon_1 \epsilon_2}{p_2 p_1} + L \left[\frac{8E_1 E_2}{3p_1 p_2} + \frac{k^2(E_1^2 E_2^2 + p_1^2 p_2^2)}{p_1^3 p_2^3} \right. \\ \left. + \frac{k}{p_1 p_2} \left(\frac{E_1 E_2 + p_1^2}{p_1^3} \epsilon_1 - \frac{E_1 E_2 + p_2^2}{p_2^3} \epsilon_2 + \frac{2kE_1 E_2}{p_2^2 p_1^2} \right) \right],$$

$$L = 2 \ln \frac{E_1 E_2 + p_1 p_2 - 1}{k},$$

$$\epsilon_1 = 2 \ln(E_1 + p_1),$$

$$\epsilon_2 = 2 \ln(E_2 + p_2),$$

$$\Delta = E_1(1 - \beta_1 \cos \theta),$$

$$Q^2 = p_1^2 + k^2 - 2p_1 k \cos \theta.$$

As is well known, Elwert¹¹ found a simple way to improve relativistic Born approximation, with a

multiplicative factor (Elwert factor)

$$f_E(\nu_1, \nu_2) = \frac{\nu_2}{\nu_1} \frac{1 - e^{-2\pi\nu_1}}{1 - e^{-2\pi\nu_2}}. \quad (2.7)$$

We have discussed elsewhere¹ some of the reasons for the success of this factor in improving the prediction of the bremsstrahlung energy spectrum $d\sigma/dk$. However, such a modification, since it is independent of angle, has no effect on the Born-approximation prediction for the shape function.

Nevertheless, the success of the Elwert-factor approach to the bremsstrahlung energy spectrum suggests that the Born-approximation prediction for the shape function is better than its prediction for the bremsstrahlung energy spectrum. As we see later in this section, this is indeed true.

Under the circumstances that $T_1, T_2 \gg 1$, Bethe and Maximon¹² obtained an analytic expression for the bremsstrahlung spectrum, justifying and using Sommerfeld-Maue¹³ wave functions for the calculation. It is believed that this calculation is valid for $T_1 > 15\text{--}50$ MeV, far above the energies currently accessible in partial-wave calculations, and consequently there is no overlap with our discussion here. More recently, Elwert and Haug¹⁴ use Sommerfeld-Maue wave functions without high-energy assumptions to obtain a result that reduces to the Sommerfeld formula for low energies, to the Bethe-Maximon formula for high energies and to the Bethe-Heitler formula for low $Z\alpha/\beta$. Since the Sommerfeld-Maue wave function is correct up to the first order in $Z\alpha$, the Elwert-Haug result is expected to fail for high Z . For the energy spectrum the Elwert-Haug approximation at intermediate (keV) energies gives predictions no better than those obtained from the Born approximation modified by the Elwert factor due to the cancellation of relativistic and higher multipole effects. However, we shall see that for angular distributions the Elwert-Haug formula is an improvement, because for light Z the approximation does remain valid at low energies and so more correctly represents the higher multipoles which contribute to

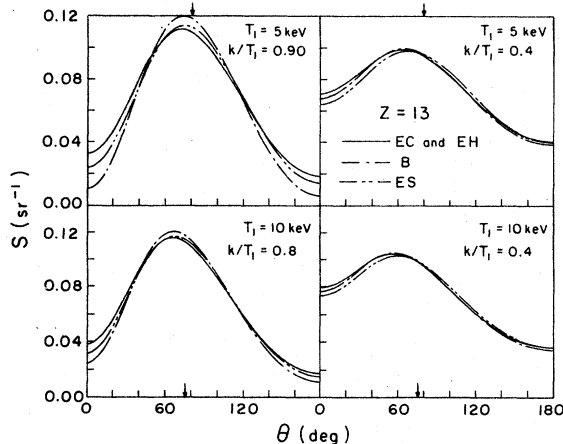


FIG. 1. Comparisons of the shape functions $S \equiv (d\sigma/dk d\Omega_p)/(d\sigma/dk)$ for Al obtained from the partial-wave method (EC for point-Coulomb potential, ES for the screened case) with the point-Coulomb results obtained from the Elwert-Haug approximation (EH) and the Born approximation (B). Note that the EH is almost the same as the EC for this low- Z case. The arrows indicate the angle for the maximum of $(d\sigma/dk d\Omega_p) \sin \theta$.

the distribution.

In Figs. 1 and 2, we present the shape functions S for a low- Z element (Al) and for a high- Z element (Au). In each panel of the figures, we make a comparison of the shape functions obtained from partial-wave calculations for a completely ionized atom (EC) and for a neutral target atom (ES) with the results obtained from the Born (B) approximation and the Elwert-Haug (EH) approximation at specified incident electron energy T_1 and fractional energy loss k/T_1 . For Al the factor $Z\alpha$ is about 0.095 and so the EH approximation gives correct predictions for the shape functions and for the energy spectrum. At $T_1 = 5$ keV and $k/T_1 = 0.9$, where $\nu_1 = 0.683$ and $\nu_2 = 2.146$, $\sigma_B/\sigma_{EC} = 0.318$ so that Born approximation fails as would be expected, while for the shape function Born approximation is accurate within about 10%, except at forward and backward angles (i.e., in the main region which contributes to the energy spectrum). Here the bremsstrahlung energy spectrum σ is defined by $\sigma \equiv \beta_1^2 (k/Z^2) (d\sigma/dk)$. At $T_1 = 5$ keV but $k/T_1 = 0.4$, $\nu_1 = 0.683$, but now $\nu_2 = 0.897$ and $\sigma_B/\sigma_{EC} = 0.809$; the Born approximation gives a still better prediction for the shape function in this lower k/T_1 case. As T_1 increases, the Born-approximation prediction becomes better, as can also be seen from Fig. 1. Furthermore, as far as the shape functions are concerned, for low- Z elements the Elwert-Haug approach is better than Born approximation.

For Au $Z\alpha$ is 0.576. Thus the Elwert-Haug and Born approximations, do not give correct predictions for the energy spectrum.² But for the shape function both EH and Born predictions are accurate within about 15%, except at forward and backward angles, as shown in Fig. 2.

The screening effect of the atomic electrons be-

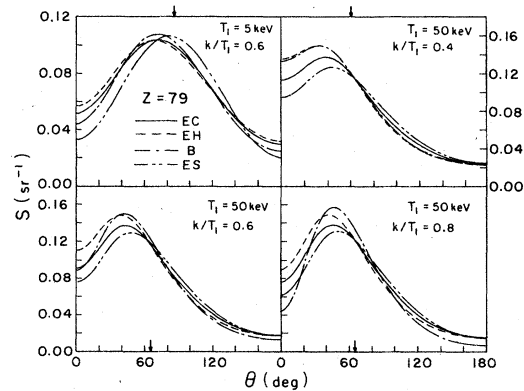


FIG. 2. Comparisons of the shape functions for Au obtained from the partial-wave method with the point-Coulomb results obtained from the Elwert-Haug approximation and the Born approximation. The arrows indicate the angle for the maximum of $(d\sigma/dk d\Omega_p) \sin \theta$.

comes important whenever the matrix element for a process involves large distances. Screening effects in bremsstrahlung change the shape function from the point-Coulomb case. From Figs. 1 and 2 we may conclude that in this range the screening effect increases as T_1 and k/T_1 decrease.

In the Born approximation¹⁵ screening results in a factor of $[1 - F(q)]^2$, which multiplies the unscreened cross section differential in photon energy and in photon and electron angles. Here $F(q)$ is the atomic form factor. Following the method of Gluckstern and Hull¹⁶ for the point-Coulomb case for handling the integration we can easily obtain in Born approximation Borie's result¹⁷:

$$\frac{k}{Z^2} \frac{d\sigma}{dkd\Omega_k} = \frac{-\alpha^3}{4\pi p_1 s_1} \int_{(s_1 - p_2)^2}^{(s_1 + p_2)^2} dq^2 \frac{[1 - F(q)]^2}{q^4} \times \left(A + \frac{GB}{D^{3/2}} + \frac{C}{D^{1/2}} \right), \quad (2.8)$$

where

$$\vec{s}_1 = \vec{p}_1 - \vec{k}, \quad \vec{q} = \vec{p}_1 - \vec{p}_2 - \vec{k},$$

$$A = \frac{4E_2^2 - q^2}{\Delta^2} + \frac{2k(q^2 + kG)}{\Delta}, \quad B = 4E_1^2 - q^2,$$

$$C = 2k^2 \Delta - 4k(E_1^2 + E_2^2)$$

$$- \frac{[2(E_1^2 + E_2^2) - q^2][2E_2^2 - s_1^2 - p_2^2 + q^2] - 4k^2}{\Delta},$$

$$G = E_2 - \frac{s_1^2 + p_2^2 - q^2}{2s_1^2} (E_2 - \Delta),$$

$$D = \frac{1}{4s_1^2} \{ [2E_2(E_2 - \Delta) - s_1^2 - p_2^2 + q^2]^2 + 4p_1^2 \sin^2 \theta \},$$

$$\Delta = E_1(1 - \beta_1 \cos \theta).$$

We will denote the shape function obtained in the Born approximation with the form factor as BF. In an *ad hoc* fashion, one can also modify the EH triply differential cross section with the same function, and integrate over scattered-electron angles, obtaining a bremsstrahlung angular distribution designated EHF. We present, in each panel of Fig. 3, a comparison of the ES, EHF, and BF shape functions for a low- Z element (Al) and a high- Z element (Au). From Fig. 3 we see that the superiority of the Elwert-Haug approximation to the Born approximation for the shape function has been reduced by the (inconsistent) use of the form-factor approach for screening. For low- Z elements the Born approximation or the Elwert-Haug approach, modified with form-factor screening, give good predictions for the shape of the angular distributions except at forward and

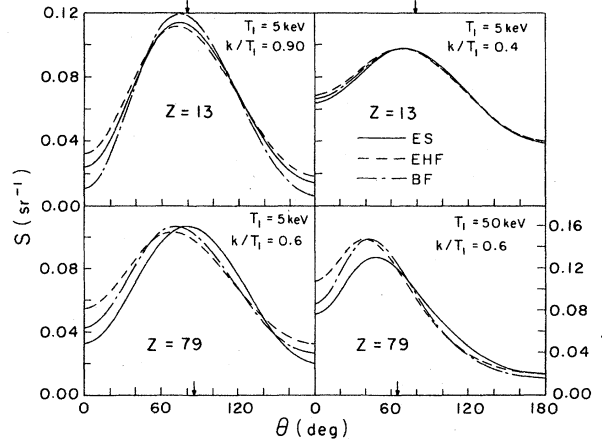


FIG. 3. Comparisons of the shape functions for neutral target atoms among the partial wave method (ES), the Elwert-Haug approximation with form-factor screening (EHF), and the Born approximation with form-factor screening (BF). The arrows indicate the angle for the maximum of $(d\sigma/dkd\Omega_k) \sin \theta$.

backward angles; while for high- Z elements, such predictions are accurate within about 15%.

In the soft-photon limit of the spectrum, as discussed by Low *et al.*,¹⁸ the bremsstrahlung matrix element is proportional to the matrix element for elastic scattering. This leads to

$$\left(k \frac{d\sigma}{dkd\Omega_k d\Omega_2} \right)_{k=0} = \left(\frac{d\sigma}{d\Omega_2} \right)_{\text{elastic}} \frac{\alpha}{4\pi^2} F, \quad (2.9)$$

where

$$F = \frac{2(1 - \vec{\beta}_2 \cdot \vec{\beta}_1)}{(1 - \hat{k} \cdot \vec{\beta}_2)(1 - \hat{k} \cdot \vec{\beta}_1)} - \frac{1}{E_2^2(1 - \hat{k} \cdot \vec{\beta}_2)^2} - \frac{1}{E_1^2(1 - \hat{k} \cdot \vec{\beta}_1)^2},$$

$$\vec{\beta}_1 \equiv \beta_1 \hat{p}_1, \quad \vec{\beta}_2 \equiv \beta_2 \hat{p}_2, \quad \beta_1 \equiv v_1/c.$$

Integrating the triply differential cross section over $d\Omega_2$, we have

$$\left(k \frac{d\sigma}{dkd\Omega_k} \right)_{k=0} = \frac{\alpha}{4\pi^2} \int \left(\frac{d\sigma}{d\Omega_2} \right)_{\text{elastic}} F d\Omega_2. \quad (2.10)$$

For the point-Coulomb case, or for high energies $(d\sigma/d\Omega_2)_{\text{elastic}}$ is strongly peaked near the forward direction. It is appropriate to expand $\vec{\beta}_2$ about $\vec{\beta}_1$ in F . Then we have

$$\left(k \frac{d\sigma}{dkd\Omega_k} \right)_{k=0} \approx \frac{A_{ij}}{(1 - \hat{k} \cdot \vec{\beta}_1)^2} + \frac{2A_{ij}\hat{k}_i\beta_{1j}}{(1 - \hat{k} \cdot \vec{\beta}_1)^3} - \frac{A_{ij}\hat{k}_i\hat{k}_j(1 - \beta_1^2)}{(1 - \hat{k} \cdot \vec{\beta}_1)^4}, \quad (2.11)$$

where

$$A_{ij} = \frac{\alpha}{4\pi^2} \int d\Omega_2 \left(\frac{d\sigma}{d\Omega_2} \right)_{\text{elastic}} (\vec{\beta}_2 - \vec{\beta}_1)_i (\vec{\beta}_2 - \vec{\beta}_1)_j.$$

If $\vec{\beta}_1$ is taken along the z axis, the only nonvanishing A_{ij} are A_{11} , A_{22} , and A_{33} , with $A_{11} = A_{22} \gg A_{33}$. Thus we have

$$S \left(\frac{k}{T_1} = 0 \right) \approx \frac{1 - \beta_1^4}{4\pi(1 - \beta_1 \cos\theta)^4} \times \left(1 - \frac{3\beta_1}{1 + \beta_1^2} P_1(\cos\theta) + \frac{1}{2} P_2(\cos\theta) \right). \quad (2.12)$$

Note that this result is already obtained in Born approximation for the point-Coulomb case.

In the screened case, the shape function in the soft-photon limit can be obtained by substituting the numerically calculated elastic scattering differential cross section $(d\sigma/d\Omega_2)_{\text{elastic}}$ into Eq. (2.10).¹⁹ In Figs. 4 and 5 we present the shape functions S at the soft-photon limit, for neutral target atoms He, O, Al, Ag, Au, U and for incident-electron energies $T_1 = 1, 10, 500$ keV. Also, in Figs. 4 and 5 we show results obtained from Eq. (2.12). From Figs. 4 and 5 we see that in the soft-photon limit: (i) Screening effects increase as T_1 and k/T_1 decrease; just as for $k/T_1 \neq 0$. (ii) At incident-electron energies below about 50 keV, the shape functions for different Z intersect each other near the "magic angles" $\theta \approx 54.74^\circ$ and 125.26° [$\cos^2\theta \approx \frac{1}{3}$, $P_2(\cos\theta) \approx \frac{5}{2} \cos^2\theta - \frac{1}{2} = 0$]. The angles of intersection vary from 57° to 50° and from 126° to 143° as T_1 varies from 1 to 50 keV. To understand this feature we note that in the nonrelativistic limit the soft-photon limit expression reduces to the NR dipole form

$$S \left(\frac{k}{T_1} = 0, \beta_1 \ll 1 \right) = \frac{1}{4\pi} [1 + A_2 P_2(\cos\theta)], \quad (2.13)$$

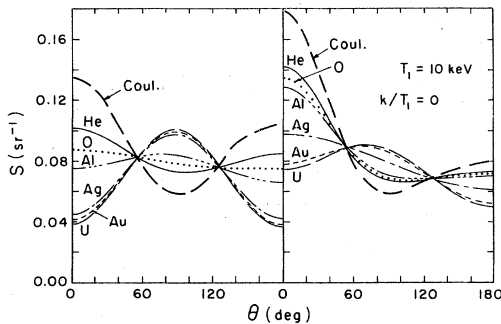


FIG. 4. Shape function at $k/T_1 = 0$ for the target atoms He, O, Al, Ag, Au, and U at incident-electron energies $T_1 = 1$ and 10 keV. The result designated as Coul is obtained from Eq. (2.12).

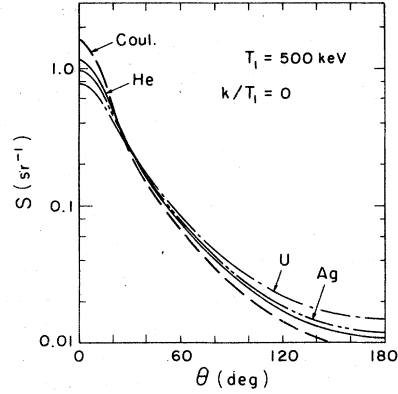


FIG. 5. Shape function at $k/T_1 = 0$ for the target atoms He, Ag, and U at $T_1 = 500$ keV. The result designated as Coul is obtained from Eq. (2.12).

where

$$A_2 = (\gamma - 1)/(1 + 2\gamma),$$

$$\gamma = b/a,$$

$$a = \frac{\alpha\beta_1^2}{4\pi^2} \int d\Omega_2 \left(\frac{d\sigma}{d\Omega_2} \right)_{\text{elastic}} (1 - \cos\theta_2)^2,$$

$$b = \frac{\alpha\beta_1^2}{4\pi^2} \int d\Omega_2 \left(\frac{d\sigma}{d\Omega_2} \right)_{\text{elastic}} (\sin\theta_2 \sin\phi_2)^2.$$

(iii) At higher T_1 this "magic-angle" feature is destroyed as shown in Fig. 5. This follows from the high-energy limit of the soft-photon limit expression. At high energies, $(d\sigma/d\Omega_2)_{\text{elastic}}$ is strongly peaked at forward angles. We have then²⁰

$$S \left(\frac{k}{T_1} = 0, \beta_1 \rightarrow 1 \right) \propto \frac{1}{(1 - \beta_1 \cos\theta)^4} (1 + A_1 P_1 + A_2 P_2), \quad (2.14)$$

where

$$A_1 = -6\beta_1\gamma/(1 + 2\gamma + 2\beta_1^2\gamma),$$

$$A_2 = (\gamma + \beta_1^2\gamma - 1)/(1 + 2\gamma + 2\beta_1^2\gamma).$$

In the point-Coulomb case, Eq. (2.14) reduces to Eq. (2.12).

Finally, in the hard-photon limit ($k/T_1 \rightarrow 1$) of the spectrum, it was first noted by Fano²¹ that there is an approximate connection between tip bremsstrahlung and atomic photoeffect. Except for normalization, reduced radial matrix elements for tip bremsstrahlung are complex conjugate to those for photoeffect. In the Sauter approximation,²² Fano obtained for tip bremsstrahlung

$$S \left(\frac{k}{T_1} \rightarrow 1 \right) \propto \frac{1}{(1 - \beta_1 \cos\theta)^4} \times \left(1 - \frac{3}{5} \frac{\delta\beta_1}{1 + \delta} P_1 - P_2 + \frac{3}{5} \frac{\delta\beta_1}{1 + \delta} P_3 \right), \quad (2.15)$$

where $\delta = \frac{1}{2} T_1(T_1^2 - 1)$. This is the same expression as obtained from the Born approximation for bremsstrahlung when $k/T_1 \rightarrow 1$.

III. REPRESENTATION AND TABULATION OF SHAPE FUNCTIONS

Convenient analytic representations are needed to facilitate systematic tabulation of the shape functions of the bremsstrahlung angular distributions. For theory as well, it is desirable to identify a small number of parameters which characterize the shape functions. One can, of course, display the shape function on some mesh in θ , which gives immediate intuitive understanding. However, effort is needed for interpolation in Z , T_1 , k/T_1 , and θ .

The "magic-angle" feature for $k/T_1 = 0$ and fixed low T_1 as Z varies is interesting and might be useful for parametrizing the shape function, but it is destroyed as k/T_1 and T_1 increase, as shown in Figs. 5 and 6. There is also a similar

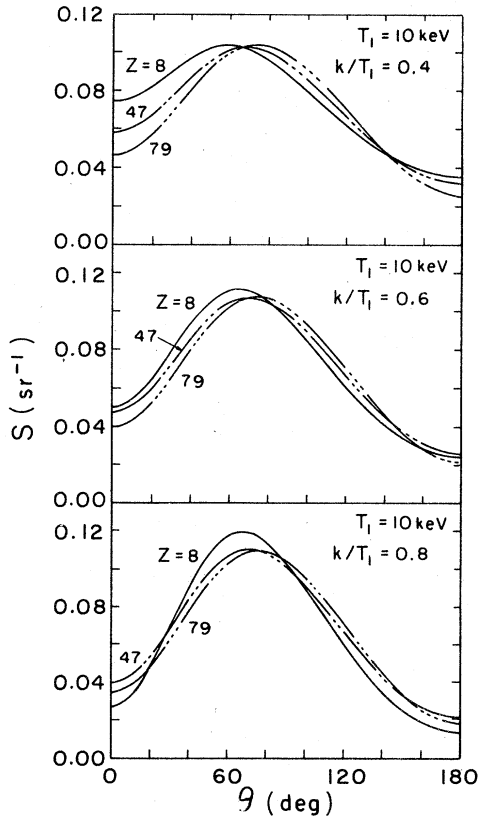


FIG. 6. Shape function at $k/T_1 = 0.4, 0.6,$ and 0.8 for various Z at $T_1 = 10$ keV.

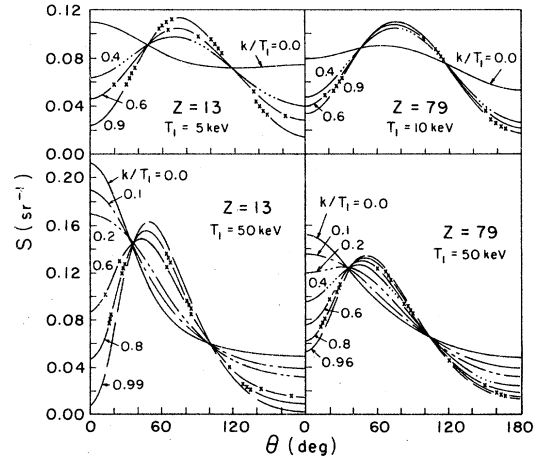


FIG. 7. Shape function for Al and Au at $T_1 = 5, 10,$ and 50 keV for various k/T_1 .

feature shown in Figs. 7 and 8, if we consider the variation of the shape function S as a function of k/T_1 at fixed Z and low T_1 . However, the two sets of angles of intersection at a fixed low T_1 are different. For example, the angles of intersection for $k/T_1 = 0, T_1 = 5$ keV as Z varies about 56° and 127° ; while for $Z = 13, T_1 = 5$ keV as k/T_1 varies are about 48° and 118° . These "magic-angle" features are interesting, but they are probably not directly useful for systematic tabulation.

Analytic properties of the shape function S from simpler theories suggest as a simple way to para-

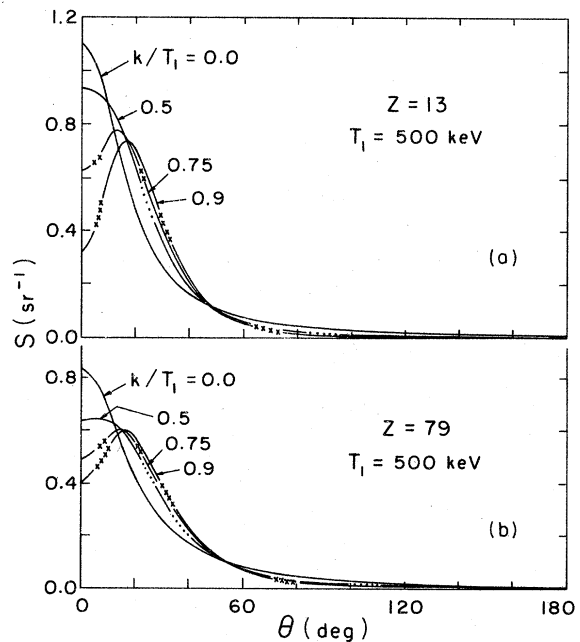


FIG. 8. Shape function for Al and Au at $T_1 = 500$ keV for various k/T_1 .

TABLE I. Expansion coefficients for $Z = 92$, $T_1 = 500$ keV, $k/T_1 = 0.6$ with the Kohn and Sham potential.

$n / B_n / m$	0	1	2	3	4
0	1.00	1.00	1.00	1.00	1.00
1	2.01	1.11	0.04	-0.80	-1.34
2	1.95	0.65	-0.09	-0.04	0.37
3	1.41	0.20	-0.18	-0.09	-0.06
4	0.83	-0.03	-0.12	0.00	0.04
5	0.37	-0.13	-0.08		0.00
6	0.06	-0.15	-0.05		
7	-0.11	-0.14	-0.03		
8	-0.19	-0.12	-0.02		
9	-0.22	-0.10	-0.02		
10	-0.22	-0.09	-0.01		

metrize the results:

$$S = \frac{A}{4\pi} \sum_{n=0}^N B_n P_n(\cos\theta) / (1 - \beta_1 \cos\theta)^m, \quad (3.1)$$

where $B_0 = 1$ and A is defined by

$$\int S d\Omega_k = 1. \quad (3.2)$$

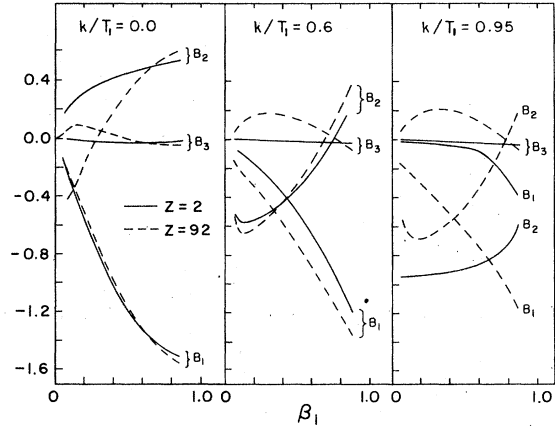


FIG. 9. B_n coefficients of the shape function in Eq. (3.1) with $m=4$ for He and U and $k/T_1 = 0, 0.6, 0.95$.

Such representations have been used to improve the convergence of partialwave series for elastic scattering.^{19,23} To illustrate the improved convergence in bremsstrahlung which can be obtained with convergence factors of the type of Eq. (3.1),

TABLE II. B_n coefficients of the shape function in Eq. (3.1) with $m=4$ calculated with the partial-wave method for $Z = 2, 8, 47, 92$, $T_1 = 1, 5, 10, 50, 100, 500$, and $k/T_1 = 0.0$ with the Kohn-Sham potential.

T_1 (keV)	Z	B_1	B_2	B_3	B_4	B_5
1	2	-0.177 92	0.172 48	-0.006 94	-0.000 82	-0.000 87
	8	-0.174 91	0.026 26	-0.001 95	-0.000 04	-0.000 02
	47	-0.162 02	-0.493 71	0.061 99	-0.003 57	0.000 16
	92	-0.163 17	-0.446 78	0.046 55	-0.001 89	0.000 03
5	2	-0.396 44	0.272 46	-0.013 23	-0.000 48	-0.000 07
	8	-0.393 08	0.210 60	-0.013 37	-0.000 30	0.000 00
	47	-0.374 78	-0.130 47	0.032 58	-0.002 41	0.000 09
	92	-0.364 29	-0.327 55	0.093 15	-0.011 47	0.001 01
10	2	-0.549 54	0.310 35	-0.016 65	-0.000 86	-0.000 09
	8	-0.546 31	0.267 46	-0.018 32	-0.000 80	-0.000 10
	47	-0.529 04	0.029 84	0.009 33	-0.001 20	0.000 03
	92	-0.514 69	-0.169 30	0.080 61	-0.013 14	0.001 23
50	2	-1.049 27	0.418 95	-0.025 51	-0.002 75	-0.000 44
	8	-1.047 80	0.405 68	-0.029 47	-0.002 96	-0.000 42
	47	-1.040 91	0.341 12	-0.032 09	-0.001 81	-0.000 10
	92	-1.027 67	0.218 44	0.020 21	-0.008 70	0.000 06
100	2	-1.267 04	0.473 89	-0.276 35	-0.003 92	-0.000 84
	8	-1.267 37	0.470 68	-0.031 17	-0.004 17	-0.000 90
	47	-1.268 19	0.451 22	-0.040 75	-0.003 04	-0.000 55
	92	-1.266 78	0.392 05	-0.018 06	-0.003 41	-0.000 74
500	2	-1.509 81	0.536 65	-0.009 86	-0.005 22	-0.001 53
	8	-1.511 83	0.539 69	-0.011 00	-0.005 28	-0.001 78
	47	-1.524 68	0.558 66	-0.017 67	-0.006 488	-0.001 93
	92	-1.563 52	0.619 67	-0.045 10	-0.004 20	-0.001 45

TABLE III. Same as Table II except that $k/T_1 = 0.6$.

T_1 (keV)	Z	B_1	B_2	B_3	B_4	B_5
1	2	-0.062 08	-0.591 62	0.006 27	0.000 66	0.000 30
	8	-0.084 48	-0.566 53	0.018 78	0.002 80	-0.000 09
	47	-0.118 85	-0.714 67	0.079 52	-0.002 68	-0.001 44
	92	-0.139 57	-0.527 29	0.052 22	-0.002 46	-0.005 12
5	2	-0.117 89	-0.573 13	-0.002 33	0.000 79	0.001 99
	47	-0.218 64	-0.603 15	0.085 56	-0.003 43	0.008 81
	92	-0.251 10	-0.652 34	0.143 09	-0.014 58	0.001 57
10	2	-0.164 70	-0.556 15	-0.004 17	0.000 37	0.000 57
	8	-0.182 92	-0.545 35	0.002 85	0.001 94	0.000 97
	47	-0.280 79	-0.536 73	0.074 98	-0.002 01	0.001 62
	92	-0.316 56	-0.624 69	0.163 45	-0.019 57	0.002 42
50	2	-0.389 62	-0.427 00	-0.007 70	0.003 54	-0.010 21
	47	-0.522 91	-0.359 24	0.041 63	0.004 43	-0.004 04
	92	-0.603 60	-0.424 11	0.163 52	-0.019 16	-0.000 43
100	2	-0.573 42	-0.291 08	-0.016 63	-0.000 70	0.002 01
	8	-0.577 75	-0.288 80	-0.015 86	0.000 65	0.002 07
	92	-0.810 05	-0.234 00	0.119 50	0.000 43	-0.005 40
500	2	-1.183 00	0.209 49	-0.013 98	0.030 02	-0.027 27
	8	-1.186 50	0.213 28	-0.014 23	0.028 41	-0.026 71
	47	-1.230 09	0.252 24	-0.022 51	0.035 69	-0.027 99
	92	-1.341 60	0.369 76	-0.060 47	0.046 44	-0.009 28

TABLE IV. Same as Table II except that $k/T_1 = 0.95$.

T_1 (keV)	Z	B_1	B_2	B_3	B_4	B_5
1	2	-0.012 02	-0.950 66	0.005 28	0.000 47	0.000 36
	8	-0.055 06	-0.774 62	0.022 43	0.002 74	0.000 08
	47	-0.125 95	-0.724 32	0.085 95	-0.004 38	0.000 88
	92	-0.164 71	-0.494 26	0.060 15	-0.004 42	0.002 50
5	2	-0.014 59	-0.946 82	-0.004 05	0.000 45	0.003 77
	47	-0.193 09	-0.690 65	0.094 25	-0.004 14	0.000 95
	92	-0.247 30	-0.678 23	0.151 71	-0.016 51	0.001 84
10	2	-0.019 55	-0.944 95	-0.001 33	-0.000 84	0.000 14
	8	-0.046 77	-0.902 85	0.008 05	0.000 88	0.000 64
	47	-0.232 36	-0.662 80	0.086 41	-0.002 19	0.001 11
	92	-0.298 57	-0.687 35	0.179 37	-0.022 65	0.002 27
50	2	-0.043 75	-0.918 30	-0.011 44	0.003 54	-0.007 34
	47	-0.336 01	-0.629 54	0.057 60	0.008 57	-0.003 45
	92	-0.524 56	-0.562 39	0.193 45	-0.019 08	-0.000 70
100	2	-0.062 77	-0.887 33	-0.027 43	-0.004 49	0.001 72
	8	-0.073 51	-0.877 19	-0.025 79	-0.003 55	0.002 12
	92	-0.679 39	-0.419 51	0.152 91	0.003 55	-0.085 30
500	2	-0.394 43	-0.581 86	-0.020 34	0.036 85	-0.037 86
	8	-0.410 33	-0.577 80	-0.006 15	0.004 62	-0.000 32
	47	-0.746 49	-0.272 28	0.002 07	0.022 95	0.001 86
	92	-1.175 52	0.186 71	-0.070 47	0.065 85	-0.001 17

we give in Table I for $Z=92$, $T_1=500$ keV, $k/T_1=0.6$, the coefficients B_n for $m=0-4$. As we can see, the best choice in this particular case is $m=3$, for which only B_1 , B_2 , and B_3 are needed to characterize S . However, in the energy range we considered the best overall choice is $m=4$; only B_1-B_5 are then needed to characterize S in this range. We show in Fig. 9 and Tables II-IV how such coefficients vary with Z , T_1 , and k/T_1 . Note that all except B_2 become small with de-

creasing energy, which is expected from nonrelativistic dipole approximation.

ACKNOWLEDGMENTS

This work was supported in part by NSF under Grant No. PHY74-03531-A03 and 01P7503599, and in part by the National Science Council, Republic of China. Dr. Simon Yu contributed several helpful suggestions.

*On leave from Department of Physics, National Central University, Chung-Li, Taiwan, Republic of China.

†Present address: Laboratory of Laser Energetics, University of Rochester, Rochester, N. Y. 14627.

¹H. K. Tseng and R. H. Pratt, Phys. Rev. A 3, 100 (1971); R. H. Pratt and H. K. Tseng, Phys. Rev. A 11, 1797 (1975).

²C. M. Lee, L. Kissel, R. H. Pratt and H. K. Tseng, Phys. Rev. A 13, 1714 (1976).

³See, for example, D. G. Brown, U. S. Department of Health, Education and Welfare Report No. BRH/DEP 70-18, 1970 (unpublished).

⁴For example, S. Von Goeler, W. Stodiek, H. Eubank, H. Fishman, S. Grebenshchikov, and E. Hinnov, Nucl. Fusion 15, 301 (1975).

⁵D. A. Liberman, D. T. Cromer, and J. T. Waber, Comput. Phys. Commun. 2, 107 (1971); W. Kohn and L. J. Sham, Phys. Rev. 140, A1133 (1965).

⁶R. M. Thaler, M. Goldstein, J. L. Mchale and L. C. Biedenharn, Phys. Rev. 102, 1567 (1956).

⁷P. Kirkpatrick and L. Wiedmann, Phys. Rev. 67, 321 (1945).

⁸A. Sommerfeld, Ann. Phys. (Leipzig) 11, 257 (1931).

⁹J. W. Motz and R. C. Placious, Phys. Rev. 109, 235 (1958).

¹⁰H. A. Bethe and W. Heitler, Proc. Soc. Lond. A 146, 83 (1934); F. Sauter, Ann. Phys. (Leipzig) 20, 404 (1934); G. Racah, Nuovo Cimento 11, 461 (1934); 11, 467 (1934).

¹¹G. Elwert, Ann. Phys. (Leipzig) 34, 178 (1939).

¹²H. A. Bethe and L. C. Maximon, Phys. Rev. 93, 768 (1954).

¹³A. Sommerfeld and A. W. Maue, Ann. Phys. (Leipzig) 22, 629 (1935).

¹⁴G. Elwert and E. Haug, Phys. Rev. 183, 90 (1969).

¹⁵H. Bethe, Proc. Cambridge Phil. Soc. 30, 524 (1934); Ann. Phys. (Leipzig) 5, 385 (1930).

¹⁶R. L. Gluckstern and M. H. Hull, Jr., Phys. Rev. 90, 1030 (1953).

¹⁷E. Borie, Nuovo Cimento A 11, 969 (1972). Note that there are misprints in Eqs. (1a), (2), (6), and (7) of this reference but Eqs. (4) and (5) are correct.

¹⁸F. E. Low, Phys. Rev. 110, 974 (1958); T. H. Barnett and N. M. Kroll, Phys. Rev. Lett. 20, 86 (1968).

¹⁹We have written a computer code to obtain the elastic scattering differential cross section with partial-wave method following the trick given in S. R. Lin, Phys. Rev. 133, A965 (1964).

²⁰Equation (2.14) reduces to Eq. (2.13) in the limit $\beta_1 \rightarrow 0$ even though the validity of Eq. (2.14) is for large β_1 . Based on classical electrodynamics one can obtain the same result as given by Eq. (2.14). See for example, J. D. Jackson, *Classical Electrodynamics*, 2nd ed., (Wiley, New York, 1975), p. 705.

²¹Y. Fano, Phys. Rev. 116, 1156 (1959).

²²F. Sauter, Ann. Phys. (Leipzig) 9, 217 (1931); 11, 454 (1931).

²³See for example, D. G. Ravenhall and R. N. Wilson, Phys. Rev. 95, 500 (1954).